# Design methodology for a special single winding based bearingless switched reluctance motor

*Madhurjya Dev Choudhury*[1], *Firdausa Ahmed*[2], *Gaurav Kumar*[1], *Karuna Kalita*[1], *Kari Tammi*[3]

[1]*Department of Mechanical Engineering, Indian Institute of Technology Guwahati, Guwahati 781039, India*
[2]*Center for Energy, Indian Institute of Technology Guwahati, Guwahati 781039, India*
[3]*Department of Mechanical Engineering, Aalto University, P.O. Box 11400, 00076 Aalto, Finland*
*E-mail: karuna.kalita@iitg.ernet.in*

Published in *The Journal of Engineering*; Received on 27th December 2016; Accepted on 5th June 2017

**Abstract:** Bearingless switched reluctance motors (BSRMs) have both magnetic bearing as well as conventional motor characteristics which make them suitable for diverse industrial applications. This study proposes a design methodology for a BSRM in order to calculate the appropriate geometrical dimensions essential for realising a minimum levitation force at every orientation of rotor. It is based on the stator–rotor overlap angle and helps in reducing the complexities associated with the self-bearing operation of a switched reluctance motor (SRM). Different from a conventional SRM, the motor under study deploys a special single set parallel winding scheme for simultaneous production of torque as well as radial force. An analytical model incorporating this single set winding is developed for calculating the torque and the radial force. The proposed bearingless design is verified by developing a two-dimensional finite-element model of a 12/8 SRM in ANSYS Maxwell.

## 1 Introduction

Bearingless switched reluctance motor (BSRM) magnetically integrates the characteristics of a conventional switched reluctance motor (SRM) with an active magnetic bearing (AMB) [1–3]. Both AMB and SRM are based on reluctance force known as the Lorentz force where a magnetic pole attracts ferritic material. AMBs enable the rotor position control using Lorentz forces. Similarly in SRMs, a torque can be produced by exerting a rotating magnetic field on a non-circular prismatic rotor.

SRM is a doubly salient electrical motor where torque is produced, by magnetic attraction between the rotor and the stator, due to the tendency of the rotor pole to achieve a minimum reluctance position. Along with the torque a considerable amount of radial force is also generated in this process. This inherent radial force provides us with an opportunity to convert a conventional SRM into a BSRM [1, 4]. The bearingless structure has the advantage of high-speed applications which is a limitation of a conventional motor supported on mechanical bearings. Thus, it is expected that a BSRM will be suitable for high-speed and maintenance-free operations under special conditions like at high temperature or in intense temperature variation [1, 5]. It also provides a new approach in solving the noise and vibration problem associated with any conventional SRM [6, 7].

Researchers have introduced several methodologies to produce torque as well as radial force in a SRM [2, 4, 6, 8–11]. The primary focus of these studies has been on the stator–rotor geometry and the winding structure. Takemoto *et al.* [4] proposed a bearingless structure of a 12/8 SRM utilising dual sets of stator winding where the main winding was responsible for producing torque and the secondary winding for providing suspension force to the rotor. However, this dual set design consumes an additional space in the stator winding which could have been otherwise used for torque production. So, researchers focused on utilising the single set winding present in a conventional SRM for generation of both the torque and the radial force [2, 9–12]. Higuchi *et al.* first proposed this idea of using single set of winding for torque and force production in SRMs in 1989 [4] and later in 1995 Preston applied it specifically for a 12/8 BSRM; however they did not publish any literature of its successful operation and control [10]. Liu and Yang [12], and Lin and Yang [11] proposed a 12/8 BSRM in which there is a single winding on each of the stator teeth. In this method, the torque is produced through conventional method by exciting all the stator teeth with equal currents in the inductance ascending phase (conduction phase) of the motor. The levitation force is generated by exciting any two teeth of the inductance descending phase. The main drawback of this scheme is that the maximum attainable radial force is limited by the torque requirement of the motor. Again Chen and Hofmann [10, 13–15] proposed an analytical model, design procedure and later experimentally implemented the idea of utilising a simpler single set stator winding for an 8/6 bearingless structure. The major contribution of this study is that it proposes a method where the total winding number of motor is decreased from eight to six in order to produce the same force and torque. They proposed a special motor driving theory and speed regulation technique where three phase windings are initially energised by different currents in each commutating period in order to produce the required force and torque.

However, the methods discussed so far are based on complex control strategies and are dependent on selecting a proper excitation scheme of the various stator pole windings of a conventional SRM geometry in order to achieve the required force and torque. Morrison [16] in 2002 patented the idea of a hybrid rotor single winding based BSRM, where he changed the structure of the SRM in order to simultaneously levitate as well as rotate the motor. In this structure [6], the rotor is composed of circular and scalloped lamination segments. The circular lamination of the rotor is used for levitation whereas the scalloped portion is used for both levitation and motoring operations. A major shortcoming in this structure along with those discussed so far is that the torque and levitation force control are coupled. Also the operating point is selected in compromise between the torque and force values and as such the entire torque and force generation regions are not fully utilised. So, in order to improve the torque and radial force characteristics Wang *et al.* [2] proposed a 8/10 prototype hybrid stator-pole SRM for obtaining constant suspension force at all positions of operation, which can be controlled independent from torque control. He improved the model proposed by Morrison [6] by increasing the torque producing stator pole arc angle of the motor, which largely reduced the negative torque. Also in this structure as the pole arc angle of the radial force

producing pole is not less than one rotor pole pitch, a constant overlap area is maintained at any rotor position resulting in a constant radial force for a particular current and number of turns. Xu *et al.* [9] proposed a novel 12/14 hybrid pole type BSRM with short flux path and no flux reversal in the stator. This new structure has an improved torque and suspension force performance as compared to the 8/10 structure. Here the torque density is increased and the decoupling degree between the torque and suspending force control is further reduced due to the short flux path without any flux reversal. The authors also proposed a 12/8 double stator BSRM structure with decoupled torque and force control. Yang *et al.* [8] proposed a new bearingless structure of a SRM with a novel rotor structure. Here the rotor pole arc angle is greater than the stator pole arc angle in order to increase the overall stator–rotor overlap area. This wider rotor pole arc design make the winding inductance curve a flat area in the inductance maximum position, thus realising decoupling control of the levitation force and torque. The idea is realised for a 12/8 double-set winding BSRM and a 12/4 single-set winding BSRM.

In this work, a novel design methodology for proper selection of the geometrical parameters that contribute towards achieving the minimum levitation force at every orientation of rotor and reduce the complexities associated with bearingless operation is presented for a special single winding SRM. The single set winding scheme considered for simultaneous production of torque and radial force in a BSRM is called bridge configured winding (BCW). It was introduced by Khoo [17] for polyphase self-bearing machines which could generate both torque and transverse force using the same winding. The nature of this winding is such that the currents responsible for producing torque is divided into two parallel paths and an isolated power supply called bridge currents in the midpoint of the path could produce a net lateral force. With no bridge current supply, the motor could operate as a normal torque producing machine. This design is an elegant development where no additional windings were used to produce the net forces like in dual set of winding. Khoo *et al.* [18] demonstrated the practical implementation of the BCW in a conventional four-pole permanent magnet motor for producing controllable transverse forces. Ahmed *et al.* [19] first proposed the use of BCW for producing controllable radial force and torque in a 12/8 SRM. Thus, it has been observed that proper structural modifications along with changing the winding excitation scheme of a SRM helps in improving the force and the torque profiles of a bearingless motor.

The paper presents a novel step-by-step design methodology for a 12/8 BSRM. This methodology is based on the stator–rotor overlap angle which has a major effect on the radial force required for self-bearing operation of the motor. It also introduces the application of a special single-set parallel winding scheme, called BCW, in a bearingless SRM for producing the torque and the radial force. An analytical model for calculating the torque and the radial force is proposed. Finally, the proposed bearingless design of the SRM is verified using a two-dimensional finite-element (FE) model developed in ANSYS Maxwell 2D.

## 2 Analysis of working of a 12/8 BSRM

The principle of force and torque generation in a BSRM is somewhat complicated as the air-gap inductance changes with the rotation of the motor resulting in a varying profile. Fig. 1 shows the unaligned and aligned positions of a rotor tooth of a BSRM. The unaligned orientation is the position of maximum torque and minimum force whereas the aligned orientation is the position of minimum torque and maximum force as shown in Fig. 2.

It is now evident that the excitation of a particular stator tooth is started at the unaligned position in order to have sufficient motoring action. However, from the perspective of the radial force, it is the position of minimum value. Again as we know that for a bearingless motor it is required to have a constant levitation force at every

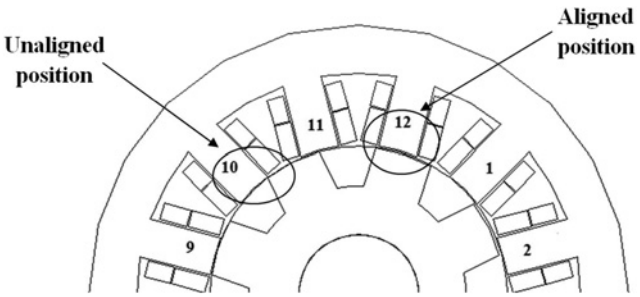


**Fig. 1** *Unaligned and aligned orientation of a BSRM*

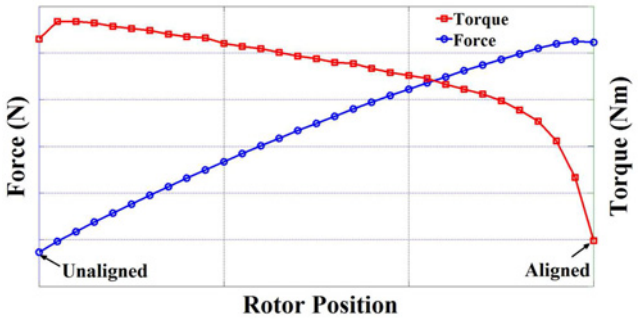


**Fig. 2** *Force and torque profiles of a single tooth of a BSRM for constant coil current*

orientation of the rotor, so the starting point of excitation ($S$) of the stator tooth has to be changed.

From the Maxwell force equation the radial force ($F$) between a stator–rotor pole can be expressed as

$$F = \frac{B^2}{2\mu_0} A_o \tag{1}$$

where $B$ is the magnetic flux density, $A_o$ is the overlap area between the rotor and the stator pole and $\mu_o$ is the permeability of free space.

Now for a constant magnetomotive force (MMF) we can make an initial approximation of the minimum area of overlap, between the rotor and the stator, required to generate the constant levitation force and accordingly decide the starting point of excitation.

Fig. 3 shows the force profile of a conventional BSRM where point $S$ is the start of excitation for a particular phase. Here the rotor rotation is started from the unaligned orientation of the rotor and is marked as 0° and this is followed for all the subsequent force and torque diagrams presented in this paper. In Fig. 3, it is observed that as we switch the excitation to the subsequent phase,

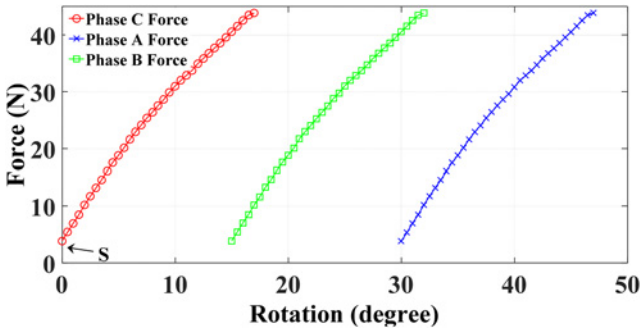


**Fig. 3** *Force profile of the various phases of a conventional BSRM for constant coil current*

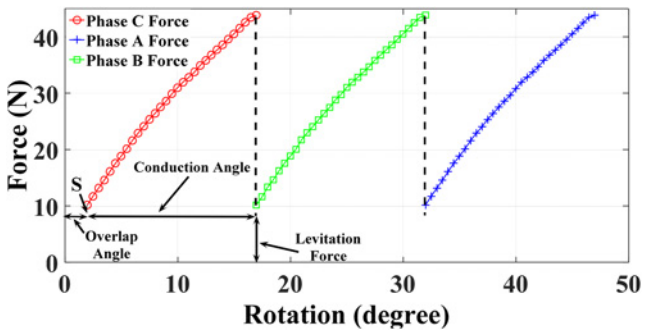


**Fig. 4** *Force profile of the various phases of a BSRM after considering the overlap angle*

the force again drops to its minimum value. Thus, at the point of switching we fail to achieve the levitation force required for bearingless operation of the motor. So in order to overcome this difficulty it is proposed to calculate the minimum stator–rotor overlap angle ($\varphi_o$) required to generate the levitation force for a particular motor and shift the excitation point $S$ to that position. It is done in order to achieve the same required levitation force after every switching. Fig. 4 shows the improved force profile at constant coil current of a single tooth of a BSRM after incorporating the effect of the overlap angle.

Moreover, on shifting the point of excitation there is a decrease in torque ripple of the motor as compared to a conventional structure. This is discussed in detail in the later sections.

## 3 Design methodology

The design procedure of a BSRM differs considerably from a conventional SRM. Due to its bearingless characteristics, more attention has to be focused on the radial force generation. This section presents a novel design methodology for a BSRM which is capable of tackling the problem described in the preceding section. For any bearingless machine, the minimum load required to levitate the rotor-shaft system plays the most important role in its design. Here based on the minimum force ($F_{\text{load}}$) required to levitate the rotor-shaft system of a SRM, the minimum stator–rotor overlap angle ($\varphi_o$) is decided for a particular MMF. Once $\varphi_o$ is fixed, the other dimensions of the motor are predicted accordingly.

Based on the procedure recommended by Vijayraghavan [20] for estimating the dimensions of a conventional SRM, the calculations are taken forward. As a good design practice, the frame size (distance from the shaft of the motor to the base) of the BSRM is first fixed by comparing it to be equivalent with an induction motor. This is done by following the IEC standards for all electrical machines made according to the International Standards Organisation (ISO) regulations [20]. Fig. 5 shows a schematic diagram of a 12/8 SRM indicating the various geometrical dimensions where $D_0$ is the outer diameter, $D$ is the inner bore diameter, $D_{\text{sh}}$ is the shaft diameter, $l_o$ is the air-gap length, $l_{\text{s}}$ and $l_{\text{r}}$ are the stator and rotor tooth lengths, $c_{\text{s}}$ and $c_{\text{r}}$ are stator and rotor back of cores. The outer diameter is calculated as

$$D_0 = 2 \times (\text{Frame size} - 3) \tag{2}$$

The 3 mm subtraction is used in industry to account for the foot of the machine, which is used for mounting. The bore diameter ($D$) is assumed to be equal to the frame size. Here the shaft diameter ($D_{\text{sh}}$) is also fixed based on the IEC standards. Before proceeding further it is important to predict the proper overlap angle and pole arc angles of the motor which has a major influence in the torque and force profiles.

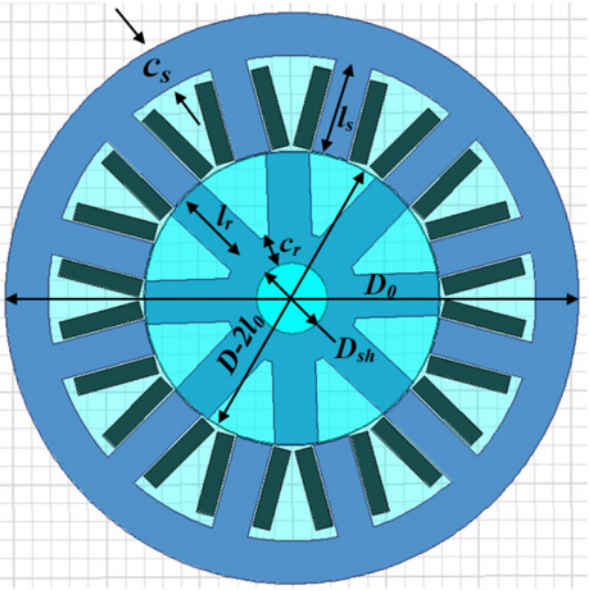


**Fig. 5** *Schematic diagram of a 12/8 SRM indicating the geometrical dimensions*

### 3.1 Selection of overlap angle

In this step, the minimum force $F_{\text{load}}$ required for a stable levitation of the rotor-shaft system of a SRM is initially estimated. Based on the $F_{\text{load}}$ required to make the SRM bearingless, the minimum stator–rotor overlap angle $\varphi_o$ is decided for a particular MMF from the equation below which is obtained after putting $B = \mu_o NI/l_o$ and $A_o = h_s r_r \varphi_o$ in (1)

$$F = \frac{\mu_0 N^2 I^2}{2l_o^2}\left(h_{\text{s}} r_{\text{r}} \varphi_o\right) \tag{3}$$

Here, $l_o$ is the air-gap length, $h_{\text{s}}$ is the motor stack length, $r_{\text{r}}$ is the rotor radius, $N$ is the number of turns of a coil and $I$ is coil current of a single tooth.

Once the overlap angle is fixed, other design variables of a SRM like the rotor and stator pole arc angles are derived based on the obtained $\varphi_o$.

### 3.2 Selection of pole arc angles

The selection of the pole arc angles is a very crucial part of the design stage of any BSRM. Unlike the previous works on calculating the pole arc angles of a BSRM, here the stator pole arc is considered to be dependent on the minimum overlap angle $\varphi_o$ as

$$\varphi_{\text{s}} = \varphi_o + \varphi_{\text{c}} \tag{4}$$

Here $\varphi_{\text{c}}$ is the conduction angle, which is the angle by which the rotor must be rotated from the position of minimum overlap $\varphi_o$ in one phase in order to obtain same overlap in the subsequent phase as depicted in Fig. 6. It is calculated as

$$\varphi_{\text{c}} = \left(\frac{2\pi}{n_{\text{r}}}\right)\frac{1}{n_{\text{ph}}} \tag{5}$$

where $n_{\text{r}}$ is the number of rotor teeth and $n_{\text{ph}}$ is the number of phases.

Fig. 6*a* shows the minimum overlap configuration for a particular phase, labelled as C, of a 12/8 SRM. Now if from this orientation the rotor is rotated by $\varphi_{\text{c}}$ degrees then it reaches the position of minimum overlap for phase A as shown in Fig. 6*b*. Thus, it is



doi: 10.1049/joe.2016.0368

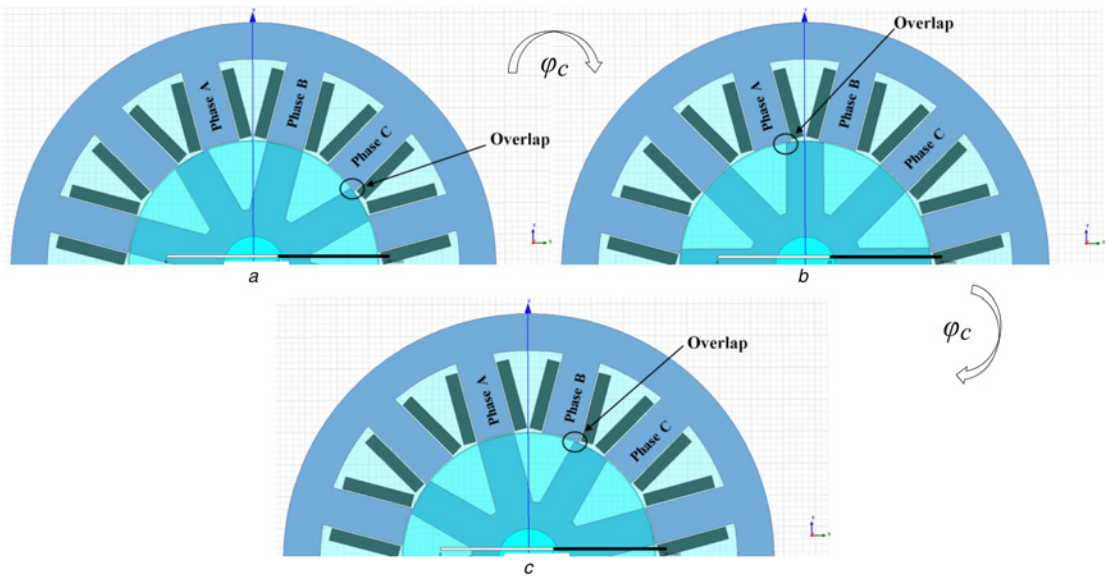


**Fig. 6** *Overlap configuration of a 12/8 SRM*
*a* Phase C overlap configuration
*b* Phase A overlap configuration
*c* Phase B overlap configuration

seen that for any rotation of the rotor, the motor is always able to achieve at least the minimum overlap angle required to generate the levitation force. Now if from the phase A overlap orientation the rotor is further rotated by $\varphi_c$ degrees then it reaches the minimum overlap orientation of phase B as shown in Fig. 6*c*. So for this particular case, the excitation sequence will start from phase C followed by phase A and phase B, respectively.

It is to be mentioned that $\varphi_o$ will always be maintained in all the phases of the motor irrespective of any combination of the stator and the rotor pole arc angles if the rotor is rotated by exactly $\varphi_c$ degrees. So as an optimum the value of the stator pole arc angle is fixed as the sum of the minimum overlap angle and the conduction angle. It is done after considering the effect of change of $\varphi_s$ on the force profile of a BSRM. Fig. 7 shows the variation of force profile at constant coil current of a single tooth of a BSRM with the change in $\varphi_s$. It is observed that for a constant rotor pole arc angle ($\varphi_r$), if $\varphi_s$ is increased then the resultant force profile increases. Thus, it is seen that a wider stator is favourable for achieving greater force for the same MMF. Here $\varphi_r$ is fixed at 15°.

Now once $\varphi_s$ is fixed, the rotor pole arc angle $\varphi_r$ is decided in the next step. It is initially chosen to be at least equal to $\varphi_s$. Choosing $\varphi_r$ smaller or greater than $\varphi_s$ also results in the same $\varphi_o$ being maintained in every phase. However, a smaller $\varphi_r$ is generally avoided for a BSRM and is kept at least equal or greater than $\varphi_s$ depending on the need. Thus

$$\varphi_r \geq \varphi_s \tag{6}$$

Moreover, if we examine the torque profile then it is observed that for a smaller $\varphi_r$ the motor is not able to maintain positive torque for full conduction of the rotor.

Fig. 8 shows the variation of torque profile at constant coil current of a single tooth of a BSRM with the change in $\varphi_r$. Here $\varphi_s$ is fixed at 17° and $\varphi_r$ is varied from 15° to 20°. Now for $\varphi_o$ = 2° and $\varphi_c$ = 15° in a three-phase 12/8 BSRM, it is observed that for $\varphi_r$ smaller than 17° the torque reaches a negative value before the rotor completes full conduction. Also from the perspective of force, like in case of variation of $\varphi_s$, an increase in $\varphi_r$ also increases the force value. Fig. 9 shows the variation of force due to the change in $\varphi_r$. Within the conduction region, it is observed that we get higher amount of force for $\varphi_r$ equal to or greater than $\varphi_s$ as compared to setting the value of $\varphi_r$ less than $\varphi_s$.

Again a larger $\varphi_r$ also results in a decrease in torque ripple of the motor. Fig. 10 shows the torque profile comparison at constant coil current between a conventional SRM and the proposed BSRM structure. It is observed that for full conduction of the motor, the torque ripple is decreased in case of a motor with $\varphi_r$ larger than $\varphi_s$.

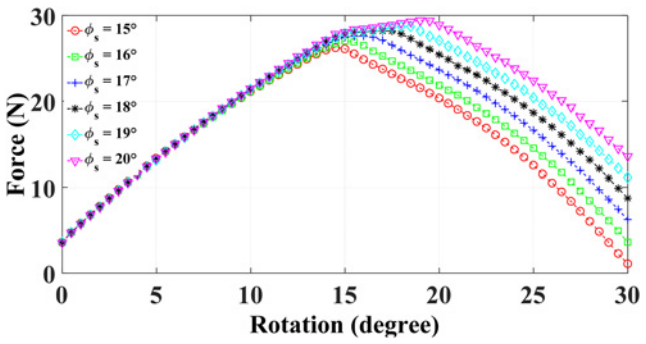


**Fig. 7** *Variation of force profiles of a BSRM due to change in $\varphi_s$*

### 3.3 Calculation of other geometrical dimensions

Once the outer diameter ($D_0$), bore diameter ($D$) and the pole arc angles are fixed for the motor, the other geometric dimensions like the stator tooth length ($l_s$), rotor tooth length ($l_r$), stator back of core ($c_s$) and rotor back of core ($c_r$) are determined for a given air gap ($l_o$) and stack length ($h_s$). From the geometry shown in Fig. 5, the stator tooth length is given by

$$l_s = \frac{D_0}{2} - c_s - \frac{D}{2} \tag{7}$$

here $c_s$ is the stator back of the core and is given by

$$c_s = \frac{A_y}{h_s} \tag{8}$$

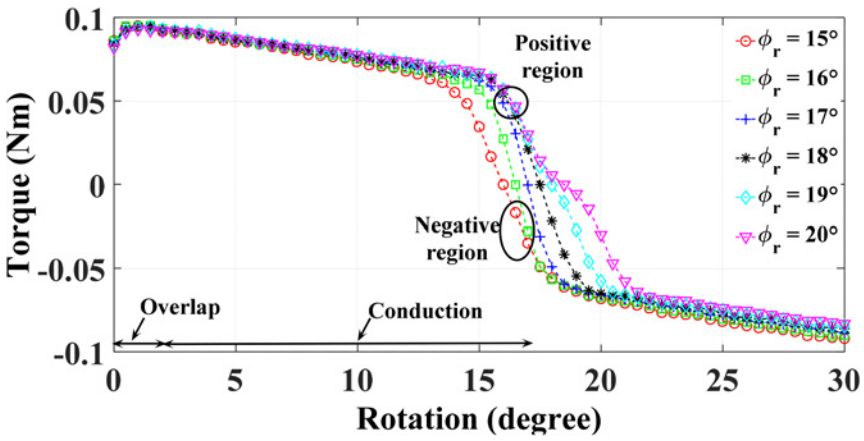


**Fig. 8** *Variation of torque profiles of a BSRM due to change in $\varphi_r$*

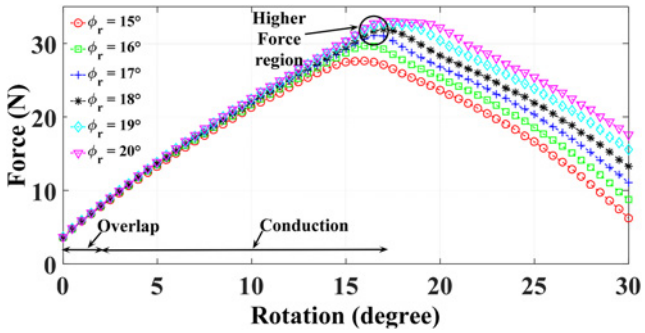


**Fig. 9** *Variation of force profiles of a BSRM due to change in $\varphi_r$*

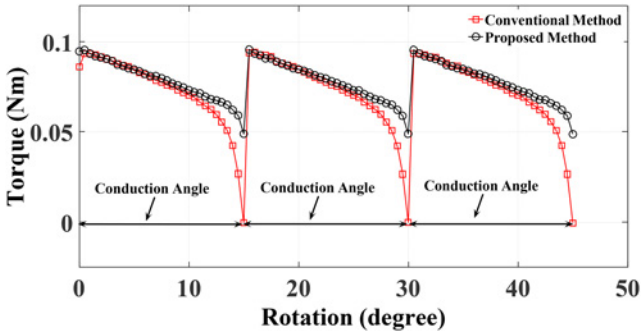


**Fig. 10** *Torque ripple comparison between a conventional SRM and the proposed BSRM structure*

Here the area of the stator back of core ($A_y$) is taken to be equal to the stator pole face area ($A_s$) assuming that back of core flux density is about half the stator pole flux density [20]. Thus

$$c_s = \frac{A_s}{h_s} \tag{9}$$

where $A_s$ is the stator pole area and is given by

$$A_s = \frac{D}{2} h_s \varphi_s \tag{10}$$

Again Krishnan [21] proposed that the rotor back of the core $c_r$ should be within the limit specified below

$$0.5\left(\varphi_s \frac{D}{2}\right) \le c_r \le 0.75\left(\varphi_s \frac{D}{2}\right) \tag{11}$$

So, the rotor tooth length is given by

$$l_s = \frac{D}{2} - c_r - \frac{D_{sh}}{2} - l_o \tag{12}$$

### 3.4 *Effect of other geometrical parameters on torque and force profiles*

The various geometrical parameters of a BSRM have direct influence on the torque and the force profiles of the motor. Out of them, the pole arc angles ($\varphi_s$ and $\varphi_r$) are found to have a major influence particularly on the force profile of the motor and it has already been discussed in detail in Section 3.3. This section

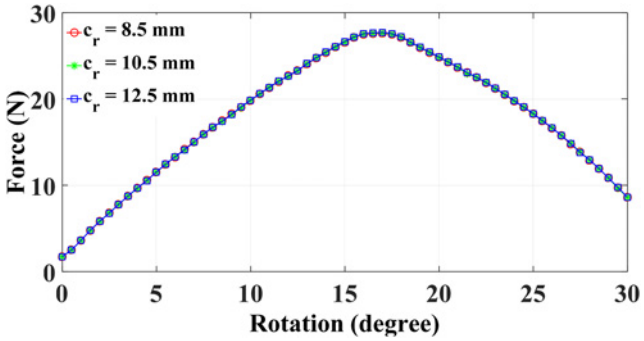


**Fig. 11** *Variation of force profiles of a BSRM due to change in $c_r$*

examines any potential influence of the other two major parameters, stator back of the core ($c_s$) and rotor back of the core ($c_r$), on the torque and the force of a BSRM. Figs. 11 and 12 show the variation of the force and the torque profiles, respectively, of a single tooth of a BSRM due to the change in $c_r$ for constant coil current.

However, no major changes are observed. Thus, it may be concluded to keep the value of $c_r$ at the nominal level as estimated in Section 3.3 as it is found to have no major influence on the force and torque profiles. Moreover, an increase in $c_r$ adds to the weight of the rotor which in turn leads to an increase of the overall levitation force requirement.

Now if the variation of force profile is examined for a change in $c_s$, it is observed that there is a very small improvement of the force with the increase in $c_s$ near the fully aligned position of the rotor.

Figs. 13 and 14 show the force and torque variations of a single tooth of a BSRM due to the change in $c_s$ for constant coil current.



doi: 10.1049/joe.2016.0368

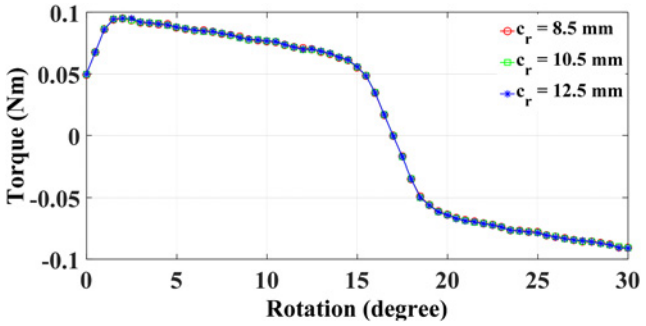


**Fig. 12** *Variation of torque profiles of a BSRM due to change in $c_r$*

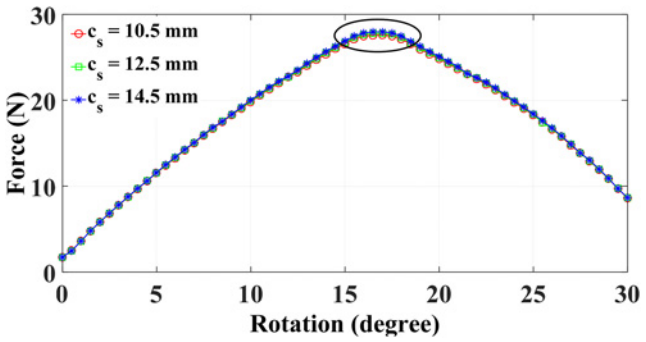


**Fig. 13** *Variation of force profiles of a BSRM due to change in $c_s$*

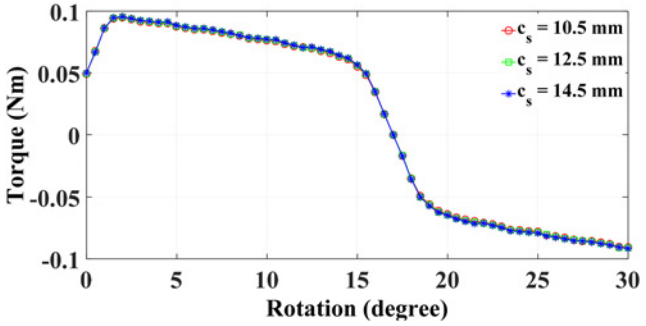


**Fig. 14** *Variation of torque profiles of a BSRM due to change in $c_s$*

As there is no major improvement in the value of force, $c_s$ may be assumed to have a value as estimated in Section 3.3.

Thus, from the above analysis it is found that the stator–rotor overlap angle and the pole arc angles ($\varphi_s$ and $\varphi_r$) are the major factors affecting the force and torque profile of a BSRM.

## 4 Introduction to bridge configured winding in a BSRM and its analytical formulation

Once the design is fixed, an attempt has been made to introduce the application of a novel single-set parallel stator winding scheme, called BCW, for producing the required radial force and torque in the BSRM. Several researchers have worked on developing an analytical model of a SRM and have made several valuable contributions [4–6, 13, 21–23]. Now in order to calculate the force and the torque of the bridge configured BSRM, a simple analytical model is developed. It is derived based on the magnetic equivalent circuit method where the force and the torque are calculated by the virtual work method as proposed by Takemoto *et al.* [4, 5]. The analytical model is developed to estimate the stored magnetic energy which is calculated from the coil inductance. The inductance is a function of the air-gap permeances which are calculated after approximating the magnetic flux lines obtained from a FE model of the motor.

### 4.1 Principle of force and torque production in a BSRM using BCW

The principle of force production using BCW in a BSRM is explained in this section. Here the currents responsible for torque production are divided into two parallel paths in each phase and an isolated supply between the midpoints of each path is utilised to generate a net radial force. Fig. 15 represents the circuit diagram of a single-phase BCW scheme, where coil sets (1a-7a′)-(7a-1a′) and (10a-4a′)-(4a-10a′) form the two parallel paths of the winding.

Fig. 16 represents the circuit and current flow diagram of a typical 12/8 bridge configured SRM. Here 1a and 1a′ constitute a coil set with same number of turns and occupy one stator tooth while coil sets 7 and 7a′ occupy diametrically opposite stator tooth, coil sets 10a-10a′ and 4a-4a′ occupy stator tooth which are 90° apart with respect to the coil sets 1a-1a′ and 7a-7a′ as shown in Fig. 16. When a current source is supplied across the point *p* and *s*, as shown in Fig. 15, magnetic field of equal magnitude is produced along the teeth 1-4-7-10, which in turn produces a torque due the tendency of the rotor to attain a state of minimum reluctance. The specialty of the BCW scheme is that with an external isolated

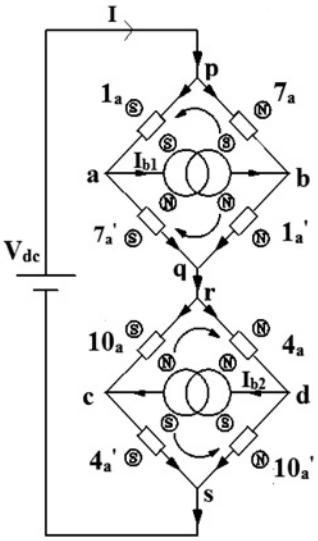


**Fig. 15** *BCW of a single phase*

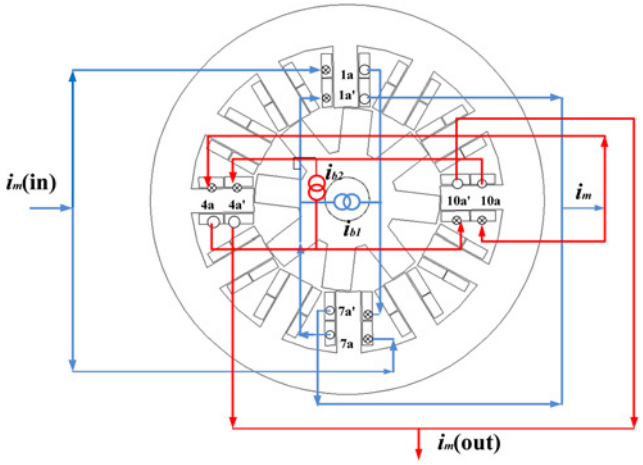


**Fig. 16** *BCW of a single phase of a typical 12/8 SRM*

supply at the bridge points (a-b) and (c-d), the symmetry in the magnetic field distribution can be disturbed, which in turn results in the generation of the radial force along with the torque. Due to this external supply across the bridge points (a, b), current flows along the paths (b-p-a and b-q-a), due to which the current density in teeth 1 increases, whereas it decreases in teeth 7. Similarly by injecting currents across points (c, d), field distribution in teeth 4 and teeth 10 can be disturbed. Thus, the need of an additional set of winding for the force production is removed.

Fig. 17*a* shows the formation of four-pole field due to the main winding current. Fig. 17*b* shows the formation of two-pole field produced due to the bridge current which is used to create asymmetry in the air gap. These bridge currents can be independently controlled and its direction can be reversed, giving rise to a net radial force in any direction.

### 4.2 Torque and radial force model

This section discusses the development of an analytical model of a bridge configured BSRM. Here the magnetic equivalent circuit method is used to approximate the inductance matrix for calculating the torque and the force. The method adopted by Takemoto *et al.* [4] is considered for calculating the air-gap permeances. However, in this present work the magnetic circuit is derived for the single-set bridge configured stator windings whereas in Takemoto *et al.* [4] it was for the dual set of windings.

Fig. 18 represents the magnetic equivalent circuit of a single phase winding superimposed on the cross-sectional view of the selected 12/8 SRM. Here, $N(i_m + i_{b1})$, $N(i_m + i_{b2})$, $N(i_m - i_{b1})$ and $N(i_m - i_{b2})$ represent the resultant MMFs at the respective teeth. The air-gap permeances are represented as resistances.

This equivalent magnetic circuit can be redrawn as shown in Fig. 19 for further analysis. The definitions of the various variables indicated in Fig. 19 are as follows: $N$ is the number of turns, $i_m$ is the main supply current, $i_{b1}$ and $i_{b2}$ are the bridge supply currents. $\phi_{a1}$, $\phi_{a2}$, $\phi_{a3}$ and $\phi_{a4}$ are the magnetic fluxes of each tooth, $P_{a1}$, $P_{a2}$, $P_{a3}$ and $P_{a4}$ are the permeances of air gaps.

Now equating the MMFs of each branches of Fig. 19 to each other we get the following equations:

$$\frac{\phi_{a2}}{P_{a2}} - N(i_m + i_{b2}) = \frac{\phi_{a1}}{P_{a1}} + N(i_m + i_{b1}) \tag{13}$$

$$\frac{\phi_{a3}}{P_{a3}} + N(i_m - i_{b1}) = \frac{\phi_{a2}}{P_{a2}} - N(i_m + i_{b2}) \tag{14}$$

$$\frac{\phi_{a4}}{P_{a4}} - N(i_m - i_{b2}) = \frac{\phi_{a3}}{P_{a3}} + N(i_m - i_{b1}) \tag{15}$$

Again, we know that the sum of magnetic fluxes through a closed surface is zero, therefore

$$\phi_{a1} + \phi_{a2} + \phi_{a3} + \phi_{a4} = 0 \tag{16}$$

Solving the MMFs equation in each branch of the circuit and using (16), the fluxes $\Phi_{a1}$–$\Phi_{a4}$ can be written in terms of permeances as

$$\phi_{a1} = -\frac{P_{a1}(P_{a2}+P_{a3}+P_{a4})}{P}N(i_m + i_{b1}) - \frac{P_{a1}P_{a2}}{P}N(i_m + i_{b2}) + \frac{P_{a1}P_{a3}}{P}N(i_m - i_{b1}) - \frac{P_{a1}P_{a4}}{P}N(i_m - i_{b2}) \tag{17}$$

$$\phi_{a2} = \frac{P_{a2}P_{a1}}{P}N(i_m + i_{b1}) + \frac{P_{a2}(P_{a1}+P_{a3}+P_{a4})}{P}N(i_m + i_{b2}) + \frac{P_{a2}P_{a3}}{P}N(i_m - i_{b1}) - \frac{P_{a2}P_{a4}}{P}N(i_m - i_{b2}) \tag{18}$$

$$\phi_{a3} = \frac{P_{a3}P_{a1}}{P}N(i_m + i_{b1}) - \frac{P_{a3}P_{a2}}{P}N(i_m + i_{b2}) - \frac{P_{a3}(P_{a1}+P_{a2}+P_{a4})}{P}N(i_m - i_{b1}) - \frac{P_{a3}P_{a4}}{P}N(i_m - i_{b2}) \tag{19}$$

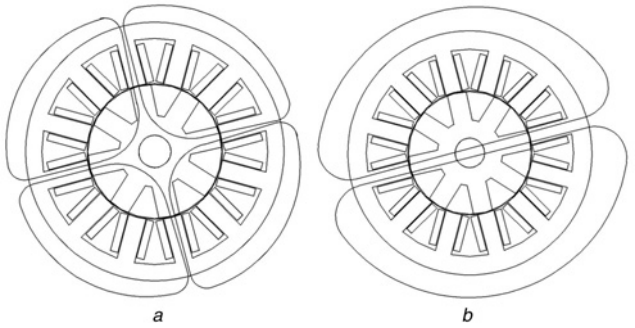


**Fig. 17** *Field formation*
*a* Four-pole field formation
*b* Two-pole field formation

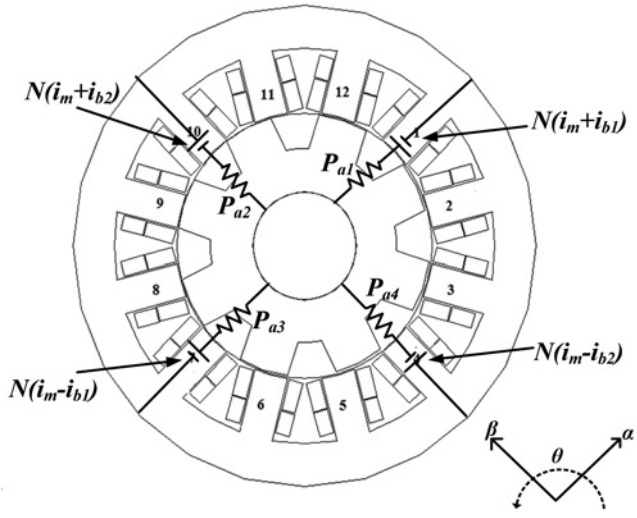


**Fig. 18** *BCW circuit of a single phase superimposed on a 12/8 SRM*

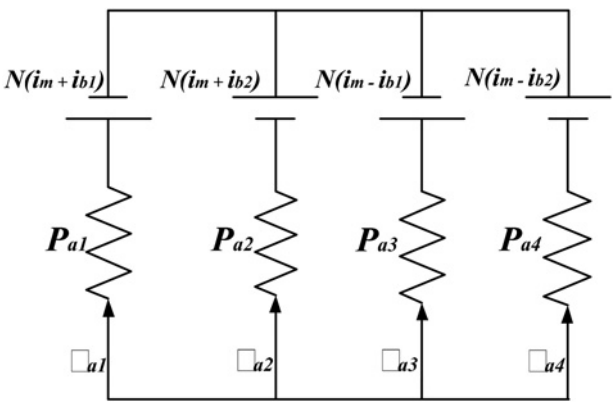


**Fig. 19** *BCW circuit diagram of a single phase*




doi: 10.1049/joe.2016.0368

$$\phi_{a4} = \frac{P_{a4}P_{a1}}{P}N(i_m + i_{b1}) - \frac{P_{a4}P_{a2}}{P}N(i_m + i_{b2}) + \frac{P_{a4}P_{a3}}{P}N(i_m - i_{b1}) + \frac{P_{a4}(P_{a1} + P_{a2} + P_{a3})}{P}N(i_m - i_{b2}) \tag{20}$$

where $P$ is the sum of all the air-gap permeances. Using the expression $N\phi = Li$, with proper sign conventions, and the equations from (17)–(20) we get the inductance matrix $[\boldsymbol{L}]$ as shown below

(see equation (21))

As it is evident from the above matrix, the inductances are a function of the air-gap permeances. The permeances are calculated based on the method proposed in [4]. It is assumed that the permeance at each stator tooth air-gap can be divided into three parts, one direct permeance and two fringing permeances. Few major assumptions considered in deriving the permeance equations are as follows:

- Magnetic saturation is neglected.
- Fringing fluxes at the aligned position are neglected as the air-gap length is very short.
- Flux paths which do not link the rotor are neglected.

The permeance of a particular air gap is given by [4]

$$P_{a1} = \left(\frac{\mu_0 h_s r_r(\theta_{\max} - \theta)}{l_0}\right) + \frac{4\mu_0 h_s}{\pi}\ln\left(\frac{4ar_r\theta + \pi l_o}{\pi l_o}\right) \tag{22}$$

The first term of the above equation is the part of permeance due to direct fluxes and the second term is due to the fringing fluxes. Here, $\theta$ is the rotor rotational position and $\theta_{\max}$ is taken to be the value of the rotor pole arc angle of the motor. Fig. 20 indicates the assumed rotor position. Again, '$a$' is a constant which is found out using finite-element method [4]. Now if no eccentricity is considered then $P_{a1} = P_{a2} = P_{a3} = P_{a4}$. Again considering radial direction displacements as $\alpha$ and $\beta$, $l_o$ is substituted by $(l_o \pm \alpha)$ and $(l_o \pm \beta)$ in (22) to get the various air-gap permeances as

$$P_{a1} = \frac{\mu_0 h_s r_r(\theta_{\max} - \theta)(l_o + \alpha)}{l_o^2} + \frac{4\mu_0 h_s}{\pi}\ln\left(\frac{4ar_r\theta(l_o + \alpha) + \pi l_o^2}{\pi l_o^2}\right) \tag{23}$$

$$P_{a2} = \frac{\mu_0 h_s r_r(\theta_{\max} - \theta)(l_o + \beta)}{l_o^2} + \frac{4\mu_0 h_s}{\pi}\ln\left(\frac{4ar_r\theta(l_o + \beta) + \pi l_o^2}{\pi l_o^2}\right) \tag{24}$$

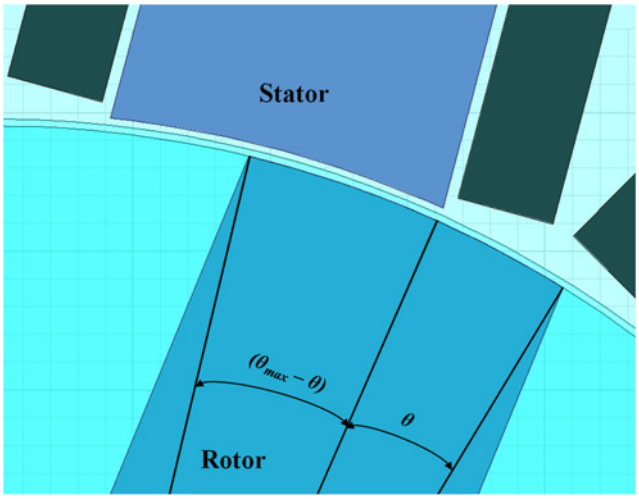


**Fig. 20** *Assumed rotor position for analytical formulation*

$$P_{a3} = \frac{\mu_0 h_s r_r(\theta_{\max} - \theta)(l_o - \alpha)}{l_o^2} + \frac{4\mu_0 h_s}{\pi}\ln\left(\frac{4ar_r\theta(l_o - \alpha) + \pi l_o^2}{\pi l_o^2}\right) \tag{25}$$

$$P_{a4} = \frac{\mu_0 h_s r_r(\theta_{\max} - \theta)(l_o - \beta)}{l_o^2} + \frac{4\mu_0 h_s}{\pi}\ln\left(\frac{4ar_r\theta(l_o - \beta) + \pi l_o^2}{\pi l_o^2}\right) \tag{26}$$

The values of the air-gap permeances are now inserted into the inductance matrix to calculate its value. Again as the stored magnetic energy, $W_a$ is half of the product of inductance and square of the current hence it can be expressed as

$$W_a = \frac{1}{2}\{i_m + i_{b1} \quad i_m + i_{b2} \quad i_m - i_{b1} \quad i_m - i_{b2}\}[L] \times \begin{Bmatrix} i_m + i_{b1} \\ i_m + i_{b2} \\ i_m - i_{b1} \\ i_m - i_{b2} \end{Bmatrix} \tag{27}$$

Here it is to be mentioned that the currents $i_m$, $i_{b1}$ and $i_{b2}$ are independent and so the current vector of (27) can be simplified further as

$$\begin{Bmatrix} i_m + i_{b1} \\ i_m + i_{b2} \\ i_m - i_{b1} \\ i_m - i_{b2} \end{Bmatrix} = \begin{bmatrix} 1 & 1 & 0 \\ 1 & 0 & 1 \\ 1 & -1 & 0 \\ 1 & 0 & -1 \end{bmatrix} \begin{Bmatrix} i_m \\ i_{b1} \\ i_{b2} \end{Bmatrix} \tag{28}$$

The torque and the radial forces are derived from the rate of change

$$[\boldsymbol{L}] = \begin{bmatrix} \frac{P_{a1}}{P}(P_{a2} + P_{a3} + P_{a4})N^2 & \frac{P_{a1}P_{a2}}{P}N^2 & -\frac{P_{a1}P_{a3}}{P}N^2 & \frac{P_{a1}P_{a4}}{P}N^2 \\ \frac{P_{a1}P_{a2}}{P}N^2 & \frac{P_{a2}}{P}(P_{a1} + P_{a3} + P_{a4})N^2 & \frac{P_{a2}P_{a3}}{P}N^2 & -\frac{P_{a2}P_{a4}}{P}N^2 \\ -\frac{P_{a1}P_{a3}}{P}N^2 & \frac{P_{a2}P_{a3}}{P}N^2 & \frac{P_{a3}}{P}(P_{a1} + P_{a2} + P_{a4})N^2 & \frac{P_{a3}P_{a4}}{P}N^2 \\ \frac{P_{a1}P_{a4}}{P}N^2 & -\frac{P_{a2}P_{a4}}{P}N^2 & \frac{P_{a3}P_{a4}}{P}N^2 & \frac{P_{a4}}{P}(P_{a1} + P_{a2} + P_{a3})N^2 \end{bmatrix} \tag{21}$$

of the stored magnetic energy as

$$T = \frac{\partial W_a}{\partial \theta} \tag{29}$$

$$F_\alpha = \frac{\partial W_a}{\partial \alpha} \tag{30}$$

$$F_\beta = \frac{\partial W_a}{\partial \beta} \tag{31}$$

The $\alpha$ and $\beta$ directions are taken to be mutually perpendicular as shown in Fig. 18. These analytical torque and force equations can be further simplified to get their relation with the currents and rotor position. However, as in our case we require the analytical model just to verify our design so the simplified form is not presented.

## 5 Validation of the proposed design

For validating the design methodology, geometry of a three-phase four-pole 12/8 BSRM is considered for an initial load ($F_{\text{load}}$)

**Table 1** Various parameters used in validating the analytical model

| Parameter | Value in mm |
|---|---|
| outer diameter of stator, $D_0$ | 154 |
| bore diameter, $D$ | 80 |
| shaft diameter, $D_{\text{sh}}$ | 19 |
| air-gap length, $l_o$ | 0.5 |
| stack length, $h_{\text{s}}$ | 100 |
| stator back of core, $c_{\text{s}}$ | 10.46 |
| rotor back of core, $c_{\text{r}}$ | 8.5 |
| stator tooth length, $l_{\text{s}}$ | 26.54 |
| rotor tooth length, $l_{\text{r}}$ | 21.5 |
| unknown parameter, $a$ | 0.9596 |

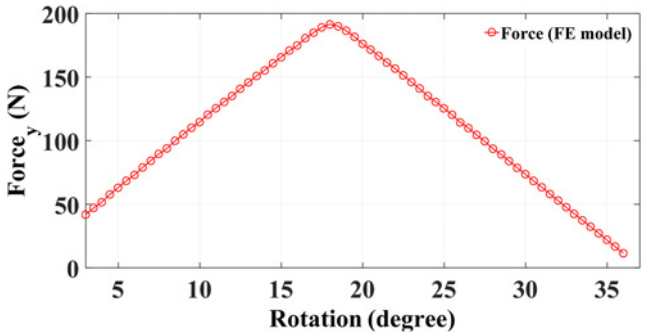


**Fig. 21** *Levitation force profile generated by the FE model of the 12/8 SRM designed based on the proposed methodology*

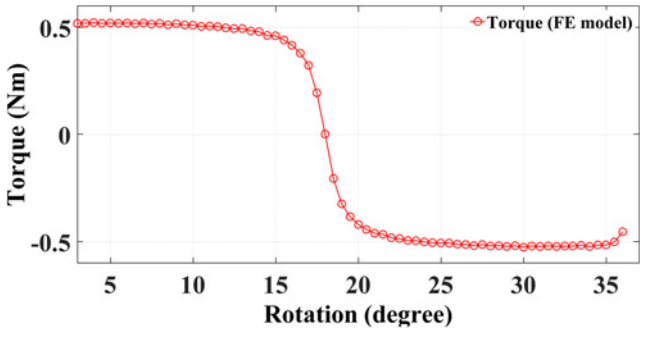


**Fig. 22** *Torque profile generated by the FE model of the 12/8 SRM designed based on the proposed methodology*

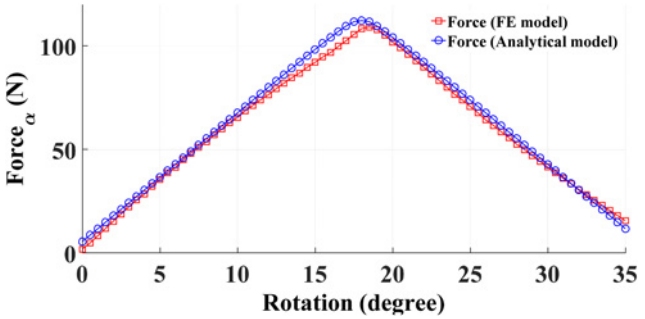


**Fig. 23** *Comparison of the α-direction force generated by the analytical model and the FE model*

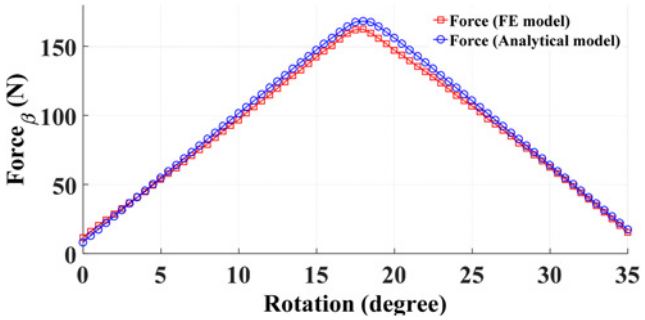


**Fig. 24** *Comparison of the β-direction force generated by the analytical model and the FE model*

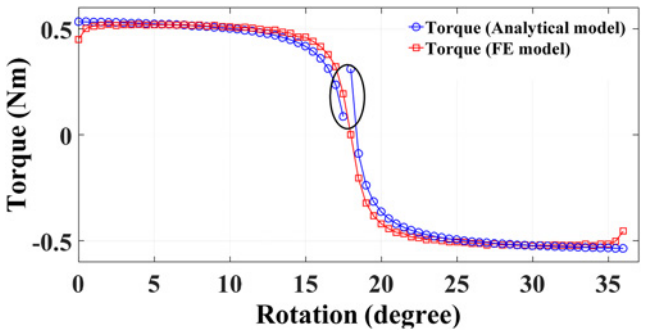


**Fig. 25** *Comparison of the torque profile generated by the analytical model and the FE model for a = 0.9596*

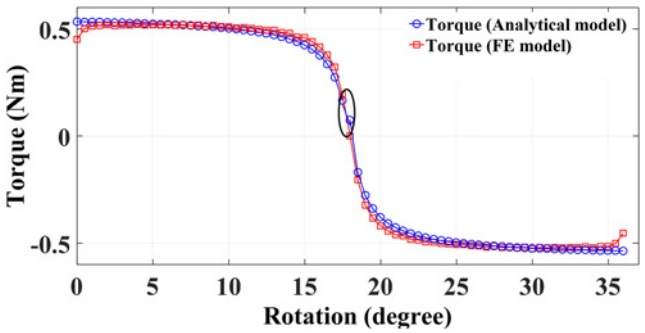


**Fig. 26** *Comparison of the torque profile generated by the analytical model and the FE model for a = 0.7*

requirement of 35 N. A minimum overlap angle ($\varphi_o$) of around 3° is determined to be maintained. It is calculated for $N = 30$ turns, $i_m = 5$, $i_{b1} = 2$ and $i_{b2} = 3$ A. The conduction angle for this particular motor is found to be 15°. So, according to the proposed design methodology $\varphi_{\text{s}}$ and $\varphi_{\text{r}}$ are taken to be 18° each.




doi: 10.1049/joe.2016.0368

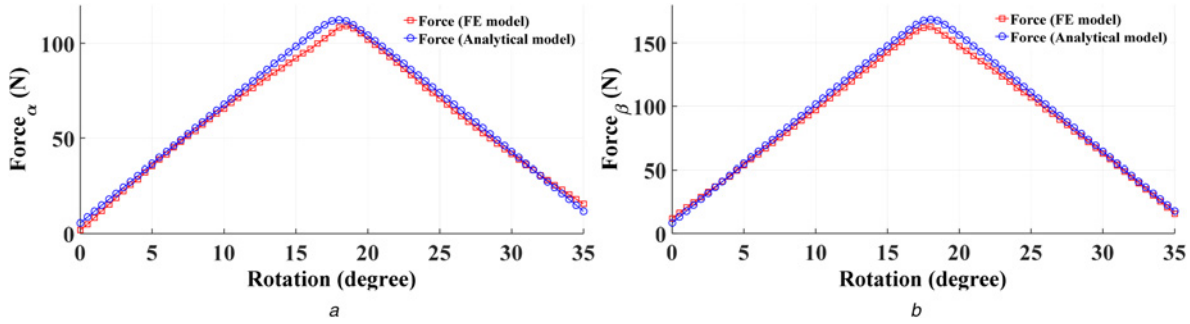


**Fig. 27** *Force profiles generated by the analytical model and the FE model*
*a* $\alpha$-direction force profiles generated by the analytical model and the FE model for $a = 0.7$
*b* $\beta$-direction force profiles generated by the analytical model and the FE model for $a = 0.7$

Table 1 provides the various dimensions of the 12/8 SRM considered for analysis. Based on these parameters, a two-dimensional FE model is developed in ANSYS Maxwell and the results obtained are utilised to validate the design methodology.

Figs. 21 and 22 show the $y$-direction force (levitation force) profile and torque profile of the motor as obtained from the FE model of the 12/8 SRM designed based on the proposed design methodology.

As per the initial estimation, a force of 35 N is expected to be generated at $\varphi_o = 3°$. The FE model is found to have a force of 41.91 N at this position, which is within acceptable limits.

The analytical torque and force models represented by (29)–(31) are solved in MATLAB and the results are compared with that obtained from the FE model of the 12/8 SRM.

Figs. 23 and 24 show the comparison of the $\alpha$-direction and $\beta$-direction force profiles as obtained from the analytical model and the FE model. The results obtained from the FE model of the 12/8 BSRM, designed based on the proposed methodology, are in good agreements of that predicted from the analytical model of the SRM. However, while verifying the torque obtained from the expression shown in (29), it is observed that at the fully aligned position of the rotor the torque values have some discrepancies. Fig. 25 shows the torque profile obtained from the FE model and the inconsistent profile obtained from the analytical model for $a = 0.9596$. This discrepancy is attributed to the fact that at the aligned position the fringing fluxes are neglected. As a result, the value of the parameter $a$, which is associated only with the fringing fluxes, fails to calculate the exact value of torque near the aligned positions.

However, it has been seen that for values of a near 0.65–0.7 the torque profile discrepancy is removed at regions near the aligned position.

So in order to improve the aligned position values of torque so that it shows agreement with the FE result, a value of $a = 0.7$ is taken. Fig. 26 shows the comparison of the corrected analytical torque profile with the results obtained from the FE model for $a = 0.7$.

It has been observed that the corrected value of '$a$' has minimal effect on the force profiles. This result is in accordance with the developed analytical model as the force is predominantly influenced by the direct fluxes as compared to the fringing fluxes. Figs. 27*a* and *b* show the $\alpha$-direction and $\beta$-direction force profiles for $a = 0.7$, respectively.

## 6 Conclusion

In this paper, a novel bearingless structure of a special single winding based 12/8 SRM is proposed. First the minimum overlap angle required to generate the levitation force for a particular MMF is approximated. It is then extended to calculate the appropriate stator and rotor pole arc angles such that we can predict a proper excitation scheme required for simultaneous motoring as well as self-bearing operation of the BSRM. A step-by-step methodology and the accompanying factors affecting the selection of the various geometrical parameters and their influence on the torque and force profiles of a BSRM are also presented in detail. It is also observed that the design suggested in this paper results in low torque ripple. An analytical model is developed to calculate the torque and the force of the bridge configured BSRM. Finally, a 2D FE model of the 12/8 BSRM, whose dimensions have been predicted based on the proposed design methodology, is considered for validation.

## 7 Acknowledgment

The authors acknowledge the Ministry of Electronics and Information Technology, Government of India.

## 8 References

[1] Chiba A., Fukao T., Ichikawa O., *ET AL.*: 'Magnetic bearings and bearingless drives' (Newnes Elsevier, 2005)
[2] Wang H., Lee D.H., Park T.H., *ET AL.*: 'Hybrid stator-pole switched reluctance motor to improve radial force for bearingless application', *Energy Convers. Manage.*, 2011, **52**, (2), pp. 1371–1376
[3] Halmeaho T., Haarnoja T., Manninen A., *ET AL.*: 'Magnetic bearing as switched reluctance motor-feasibility study for bearingless switched reluctance motor'. Proc. IEEE Int. Electric Machines & Drives Conf., USA, 2013, pp. 401–408
[4] Takemoto M., Shimada K., Chiba A.: 'Design and characteristics of switched reluctance type bearingless motors'. Proc. 4th Int. Symp. Magnetic Suspension Technology, Japan, 1997, pp. 49–63
[5] Takemoto M., Chiba A., Akagi H., *ET AL.*: 'Radial force and torque of a bearingless switched reluctance motor operating in a region of magnetic saturation', *IEEE Trans. Ind. Appl.*, 2007, **40**, (1), pp. 103–112
[6] Morrison C.R., Siebert M.W., Ho J.E.: 'Electromagnetic forces in a hybrid magnetic-bearing switched-reluctance motor', *IEEE Trans. Magn.*, 2008, **44**, (12), pp. 4626–4638
[7] Yuan Y., Sun Y., Huang Y.: 'Radial force dynamic current compensation method of single winding bearingless flywheel motor', *IET Power Electron.*, 2015, **8**, (7), pp. 1224–1229
[8] Yang Y., Liu Z., Deng Z., *ET AL.*: 'Design and characteristic analysis of a novel bearingless SRM considering decoupling between torque and suspension force', *Math. Probl. Eng.*, 2014, **2014**, pp. 1–12
[9] Xu Z., Lee D.H., Ahn J.W.: 'Comparative analysis of bearingless switched reluctance motors with decoupled suspending force control', *IEEE Trans. Magn.*, 2015, **51**, (1), pp. 733–743
[10] Chen L., Hofmann W.: 'Speed regulation technique of one bearingless 8/6 switched reluctance motor with simpler single winding structure', *IEEE Trans. Ind. Electron.*, 2012, **59**, (6), pp. 2592–2600
[11] Lin F.C., Yang S.M.: 'Self-bearing control of a switched reluctance motor using sinusoidal currents', *IEEE Trans. Power Electron.*, 2007, **22**, (6), pp. 2518–2526
[12] Liu W.T., Yang S.M.: 'Modeling and control of a self-bearing switched reluctance motor'. Proc. 14th IAS Annual Meeting, Hong Kong, 2005, pp. 2720–2725
[13] Chen L., Hofmann W.: 'Analytically computing winding currents to generate torque and levitation force of a new bearingless switched

reluctance motor'. Proc. 12th Int. Power Electronics and Motion Control Conf., Slovenia, 2006, pp. 1058–1063
[14] Chen L., Hofmann W.: 'Design procedure of bearingless high-speed switched reluctance motors'. Proc. Int. Symp. Power Electronics, Electrical Drives, Automation and Motion, Pisa, 2010, pp. 1442–1447
[15] Chen L., Hofmann W.: 'Modelling and control of one bearingless 8/6 switched reluctance motor with single layer of winding structure'. Proc. 14th European Conf. on Power Electronics and Applications, Birmingham, 2011, pp. 1–9
[16] Morrison C.R.: 'Bearingless switched reluctance motor'. US Patent, US6727618 B1, April 2004
[17] Khoo W.K.S.: 'Bridge configured winding for polyphase self-bearing machines', *IEEE Trans. Magn.*, 2005, **41**, (4), pp. 1289–1295
[18] Khoo W.K.S., Kalita K., Garvey S.D.: 'Practical implementation of the bridge configured winding for producing controllable transverse forces in electrical machines', *IEEE Trans. Magn.*, 2011, **7**, (6), pp. 1712–1718
[19] Ahmed F., Kumar G., Choudhury M.D., *ET AL.*: 'Bridge configured wounded switched reluctance motor', *Proc. Eng.*, 2016, **144**, pp. 817–824
[20] Vijayraghavan P.: 'Design of switched reluctance motors and development of a universal controller for switched reluctance and permanent magnet brushless DC motor drives'. PhD thesis, Virginia Polytechnic Institute and State University, 2001
[21] Krishnan R.: 'Switched reluctance motor drives: modelling, simulation, analysis, design, and applications' (CRC Press, 2001)
[22] Radun A.: 'Analytical calculation of the switched reluctance motor's unaligned inductance', *IEEE Trans. Magn.*, 1999, **35**, (6), pp. 4473–4481
[23] Radun A.: 'Analytically computing the flux linked by a switched reluctance motor phase when the stator and rotor poles overlap', *IEEE Trans. Magn.*, 2000, **36**, (4), pp. 1996–2003